Smart Structures and Systems, *Vol. 34, No. 1 (2024) 51-62*
https://doi.org/10.12989/sss.2024.34.1.051

Pore network approach to evaluate the injection characteristics of biopolymer solution into soil

Jae-Eun Ryou [1a], Beomjoo Yang [1b], Won-Taek Hong [2c] and Jongwon Jung*[1]

[1] *School of Civil Engineering, Chungbuk National University, 1, Chungdae-ro, Seowon-gu, Cheongju-si, Chungcheongbuk-do, Republic of Korea*
[2] *Department of Civil & Environmental Engineering, Gachon University, 1342, Seongnam-daero, Sujeong-gu, Seongnam-si, Gyeonggi-do, Republic of Korea*

(*Received May 12, 2024, Revised August 14, 2024, Accepted August 21, 2024*)

Abstract. Application of biopolymers to improve the mechanical properties of soils has been extensively reported. However, a comprehensive understanding of various engineering applications is necessary to enhance their effectiveness. While numerous experimental studies have investigated the use of biopolymers as injection materials, a detailed understanding of their injection behavior in soil through numerical analyses is lacking. This study aimed to address this gap by employing pore network modeling techniques to analyze the injection characteristics of biopolymer solutions in soil. A pore network was constructed from computed tomography images of Ottawa 20-30 sand. Fluid flow simulations incorporated power-law parameters and governing equations to account for the viscosity characteristics of biopolymers. Agar gum was selected as the biopolymer for analysis, and its injection characteristics were evaluated in terms of concentration and pore-size distribution. Results indicate that the viscosity properties of biopolymer solutions significantly influence the injection characteristics, particularly concerning concentration and injection pressure. Furthermore, notable trends in injection characteristics were observed based on pore size and distribution. Importantly, in contrast to previous studies, meaningful correlations were established between the viscosity of the injected fluid, injection pressure, and injection distance. Thus, this study introduces a novel methodology for integrating pore network construction and fluid flow characteristics into biopolymer injections, with potential applications in optimizing field injections such as permeation grouting.

Keywords: biopolymer injection; permeation grouting; pore network model; pore-size distribution; shear-thinning fluid flow

1. Introduction

Chemical soil stabilization methods involve strengthening soil through chemical reactions. Materials such as cement, asphalt, lime, and polymers are used in these techniques (Butt *et al*. 2016, Firoozi *et al*. 2017, Lazo *et al*. 2024). However, traditional stabilizers, such as cement and asphalt, exhibit significant environmental effects that are directly associated with greenhouse gas emissions. For instance, studies have indicated that cement production accounts for approximately 8% of CO_2 emissions (Chang and Cho 2019). Moreover, the use of cement results in environmental issues such as soil alkalinization. Therefore, the civil engineering industry must develop sustainable and environment-friendly ground reinforcement materials (Mekonnen *et al*. 2022, Pushpakumara and Mendis 2022, Gidebo *et al*. 2023, Zivari *et al*. 2023).

Biopolymers, which are derived from renewable resources, offer sustainable and environment-friendly alternatives to conventional stabilizers. Moreover, owing to their biodegradability, environmental impacts are minimized after utilization (Fatehi *et al*. 2021). Soil treatment using biopolymers involves the formation of biopolymer gels and networks within the pores, which ensures the superior mechanical performance of the soil through interparticle cross-linking (Bouazza *et al*. 2009, Chang and Cho 2019). The use of biopolymers for soil treatment has been shown to enhance soil strength and permeability and promote vegetation (Soldo *et al*. 2020, Toufigh and Ghassemi 2020).

Research on actual field-based biopolymer applications for reducing the cyclic loading on road pavements, ensuring slope stability, and utilizing biopolymers as ground-injection materials has been reported (Arab *et al*. 2019, Seo *et al*. 2021, Lee *et al*. 2021). Among these works, studies related to the use of biopolymer solutions for ground injection have analyzed the required injection pressures, enhancement of injection performance owing to shear-thinning behavior, and high-temperature injection techniques utilizing sol-gel transition (Lee *et al*. 2021, Ryou and Jung 2022, 2023). Particularly, the utilization of biopolymers for improving soil permeability suggests their potential as ground-injection materials.

*Corresponding author, Ph.D., Professor,
E-mail: jjung@chungbuk.ac.kr
[a] Post-Doctoral Researcher
[b] Associate professor
[c] Assistant professor

ISSN: 1738-1584 (Print), 1738-1991 (Online)

The current research on the injection characteristics of biopolymers indicate that biopolymers enhance the mechanical performance of treated soils. However, challenges persist in the quantitative analysis while considering the non-Newtonian fluid properties of biopolymers, analysis of injection characteristics based on varying soil conditions, and numerical analytical approaches for analyzing biopolymer injection characteristics.

To address these gaps, we conducted pore network modeling by considering the viscosity characteristics of agar gum solution. A pore network model was constructed using computed tomography (CT) images of Ottawa 20-30 sand. The injection characteristics of the agar gum solution were analyzed with respect to concentration and soil conditions. Furthermore, the correlation between the viscosity properties of the injected fluid and injection characteristics is discussed.

2. Literature review

This section reviews experimental studies on the injection characteristics of biopolymers within the soil, analytical studies on the injection characteristics of other injection materials, and pore network modeling.

2.1 Injection characteristics of biopolymer solutions into porous media

Lee *et al*. (2021) evaluated the injection performance of xanthan gum biopolymer using apertures and glass beads. The injection experiments considered various injection pressures, biopolymer concentrations, and flow channel shapes. The results revealed a significant dependence of the injection efficiency of the xanthan gum biopolymer on the injection pressure and geometric properties of the pore structure; moreover, a decrease in the injection efficiency was observed with increasing biopolymer concentration. Ryou and Jung (2022) used a micromodel to evaluate the injection performances of sodium alginate and guar gum biopolymers. The viscosities of the biopolymer solutions were measured, and the penetration characteristics were analyzed using micromodel injection experiments. The findings indicated shear-thinning behavior in all biopolymer solutions, with the guar gum solution exhibiting a higher injection volume than the sodium alginate solution, which is attributable to the material properties of the individual biopolymers. Ryou and Jung (2023) conducted micromodel injection experiments under high-temperature conditions to analyze the injection characteristics of a thermo-gelation biopolymer solution. The physical properties of agar and gellan gum, such as viscosity, interfacial tension, and contact angle, were evaluated, and their impacts on fluid flow through porous media were analyzed. The results showed that the thermo-gelation biopolymer has a higher viscosity and contact angle than water, resulting in a lower capillary pressure. Moreover, variations in the viscosity, contact angle, and interfacial tension led to an increase in the injection volume with increasing concentration, demonstrating a stable displacement injection pattern. Conversely, the required injection pressure increased with increasing viscosity, owing to the increased concentration. These results highlight the inverse relationship between injection volume and pressure based on the material properties of biopolymer solutions along with the advantage of low-viscosity characteristics during high-temperature injection and potential for effective ground reinforcement through sol-gel transition. The injection efficiency of biopolymers within the soil depends on the injection pressure and geometric properties of the pore structure. The shear-thinning properties of biopolymers can induce a decrease in viscosity, highlighting their potential for enhancing the injection performance. However, quantitative analysis of these characteristics in biopolymer injections remains insufficient.

2.2 Numerical approach to assess penetration distance of conventional grout materials

Fu *et al*. (2019) proposed a mathematical model for injection grouting and conducted an analysis considering the self-gravity effect of the grout. The model, based on the generalized Darcy's law and spherical diffusion theory, was developed for the following three types of grouts: Newtonian and non-Newtonian fluids (Bingham and power-law fluids). A model predicting the penetration and diffusion behavior of the grout was also developed and validated through experiments. The experimental results indicated that the grout diffusion radius increases with decreasing injection pressure. Particularly, the power-law grout showed minimal influence on the diffusion radius when considering the grout gravity, whereas the Bingham and Newtonian grouts demonstrated more distinct effects of gravity. Coskun and Tokdemir (2020) presented a numerical model for injection grouting, targeting fully saturated soil. They simulated the simultaneous flow of grout and existing water based on immiscible multiphase fluid flow theory. The research findings indicated the effectiveness of the proposed mathematical model-based numerical simulations under saturated soil conditions. Wang *et al*. (2022) utilized a cylindrical diffusion model with a curved tube geometry to consider the geometric characteristics for modeling injection grouting. The results showed that the diffusion model incorporating curved tubes can more accurately predict the injection behavior of grout than the existing models. Variables such as grouting pressure, viscosity, and permeability coefficient were identified as the key factors influencing the injection characteristics of the grout.

Traditional injection materials exhibit dominant effects on the injection characteristics within the soil, such as grouting pressure, viscosity, and permeability coefficient. However, the numerical analysis of the injection characteristics of novel materials such as biopolymers remains insufficient.

2.3 Pore network approach to analyze fluid flow in porous media

Sochi (2010) analyzed the flows of Newtonian and non-Newtonian fluids in porous media, including shear-thinning, shear-thickening, and Bingham plastic fluids. The analysis revealed that non-Newtonian fluids exhibit time-

independent behavior, where the strain depends on the instantaneous stress, whereas time-dependent fluids express the strain as a function of the stress magnitude and duration. Moreover, viscoelastic fluids exhibit partial elastic recovery and dependence on both time and strain. They provided theoretical formulations of these characteristics, suggesting the effective utilization of continuum, capillary bundle, and pore network models to describe their flow behavior. Jithin *et al*. (2018) analyzed the influence of geometric variables on determining the scaling factors necessary for modeling the apparent viscosity of non-Newtonian fluids in porous media based on pore network structures. They simulated flows using the lattice Boltzmann method with idealized porous media structures in circular or square arrays. The apparent viscosity of non-Newtonian fluids was determined based on the computed shear rate within the pores. The analysis showed a strong correlation between the scaling factor and tortuosity, permeability, and porosity of the pores. Li *et al*. (2024) performed pore network modeling to estimate the soil–water characteristic curve. Unlike previous models, they estimated the curve based on the initial moisture content, stress hysteresis, temperature, and salinity. The pore characteristics were determined through idealization. The results showed the accuracy of the predictions through a comparison with the soil–water characteristic curves obtained from preceding experiments under different factors. They indicated the need for validation through experimental and modeling comparisons using the same sample as a limitation.

Various theoretical approaches have been used to interpret the flows of Newtonian and non-Newtonian fluids (Chen *et al*. 2022). The utilization of continuum, capillary bundle, and pore network models is feasible for analyzing the fluid flow within pores. Among these, pore network modeling offers the advantage of a relatively clear consideration of the geometric characteristics of the pores. An analysis of the injection characteristics using pore network modeling indicated their dependence on factors such as porosity, permeability, and tortuosity of the sample. However, research on the injection characteristics of biopolymers has been insufficient.

3. Pore network modelling

Pore network modeling can be effectively utilized for analyzing fluid flow within pores (Xiong *et al*. 2016). To achieve effective pore network modeling, an understanding of the complex geometric characteristics of the pores and modeling process is required. Therefore, in this section, pore extraction and fluid flow simulations are described.

3.1 Pore extraction

Ottawa sand is primarily acquired from Ottawa, Illinois, and naturally exhibits a round shape. In this study, pore network modeling was performed using original images of Ottawa sand, as described by Fei *et al*. in their study (Fei *et al*. 2021). The Ottawa sand used in this study refers to samples passing through a #20 sieve (850 μm) and retained on a #30 sieve (600 μm). These samples are representative

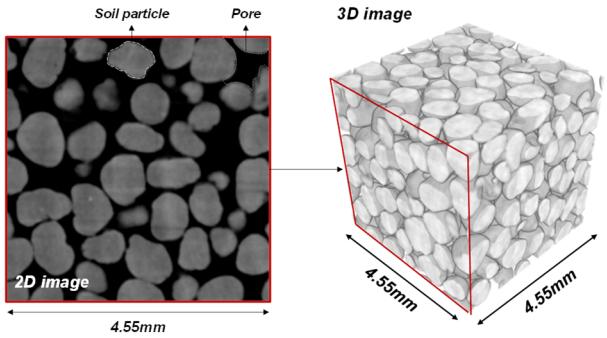

Fig. 1 Computed tomography (CT) images of Ottawa 20-30 sand (raw images were obtained from the paper published by Fei *et al*. (2021)

Table 1 Physical properties of Ottawa 20-30 sand

Sample	Height [mm]	Length [mm]	Pixel size [mm]	D50 [mm]	Particle size range [mm]	Porosity [%]
Ottawa sand	4.55	4.55	0.013	0.73	0.60-0.85	41.27

of the sands that are commonly used in geotechnical research and are characterized by smooth particle surfaces (Fei *et al*. 2021). Furthermore, the uniformity of Ottawa sand can provide consistency in experiments and simulations. For these reasons, the CT images of Ottawa sand were used in this study. The regions of interest in the original images were composed of rectangular shapes with horizontal and vertical dimensions of 4.5 mm, with a pixel size of 13 μm. The 2D and 3D of the original images are shown in Fig. 1. The physical properties of Ottawa sand are summarized in Table 1.

Original sample images may be subject to errors owing to various factors, including contrast brightness, distortion, differences in sensor component quality, and environmental conditions during image acquisition (Kim *et al*. 2022, Lee *et al*. 2024). Therefore, the original images were processed through multiple image processing stages to accurately extract the pores from these images. This process involves contrast adjustment, segmentation, and binarization. In the first stage, contrast adjustment was performed by generating a standard histogram based on grayscale values and then adjusting the histogram of individual images to match this standard (Čapek *et al*. 2006). Subsequently, segmentation was performed on the contrast-adjusted images. This process involved skeletonization and contour separation to clearly differentiate between the solid regions and pores of the sample. The segmented images were then subjected to binarization to distinctly separate the pores and solid regions.

Considering the potential for errors in the image processing, the porosity values of the samples before and after image processing were compared. Through this comparison, a threshold with an error of no greater than 0.5% was determined. Subsequently, to extract the pore network, the central axis and maximum inscribed sphere algorithms were applied. The algorithm used in this study

employed a two-step search method to determine the nearest solid particle rather than growing the sphere layer by layer (Dong and Blunt 2009). Using this approach, parameters such as pore throat size, pore body size, and pore connectivity were obtained as outputs. The overall process of the pore network extraction used in this study is illustrated in Fig. 2.

The results of pore extraction are characterized by pore throat, body, and connectivity, which collectively govern fluid behavior within the medium. The pore throat influences permeability by controlling fluid flow between pore bodies, with smaller throats restricting movement and larger throats facilitating it. Pore bodies determine fluid storage and flow paths based on their size and shape. Pore connectivity, or the degree of interconnection between pore bodies through throats, impacts overall permeability, with higher connectivity enhancing fluid movement and lower connectivity reducing it. The results of the pore network extraction from images of Ottawa sand are shown in Fig. 3. Figs. 3(a) and (b) illustrate the diameter and length distributions of pore throats, respectively, and Figs. 3(c) and (d) show the diameter and connectivity of the pore bodies, respectively. The maximum, minimum, and average diameter of pore throats were calculated as 27.7, 0.9, and 9.5 μm, respectively, with the majority of pores exhibiting pore throat diameters in the range of 6 to 8 μm. The maximum, minimum, and average length of pore throats were calculated as 236.5, 4.8, and 101.0 μm, respectively, while lengths in the range of 100 to 110 μm are frequently observed. Moreover, the lengths of the pore throats were approximately 10 times their diameters. The maximum, minimum, and average diameter of pore bodies were calculated as 100.0, 3.1, and 18.3 μm, respectively, with the maximum pore bodies having diameters in the range of 35.0 to 37.5 μm. The maximum, minimum, and average connectivities of the pores were calculated to be 10, 5.4, and 1.0, respectively, with the distribution showing the highest frequency for pores with a connectivity of 2. The extracted pore network is shown in Fig. 4.

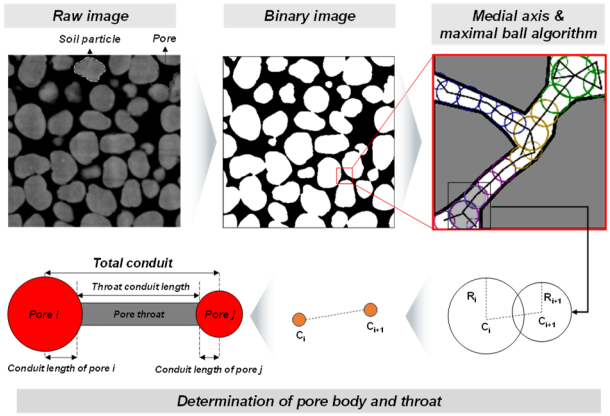

Fig. 2 Pore extraction process from CT images

3.2 Fluid flow simulation

The pore network comprises pore bodies and throats. The input parameters for the model included the spatial coordinates, diameters of pore bodies and throats, lengths of pore throats, connectivity of each pore body, injection pressure, and physical properties of both the injected and

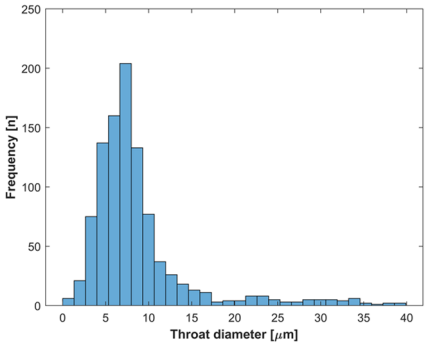

(a) Pore throat diameter

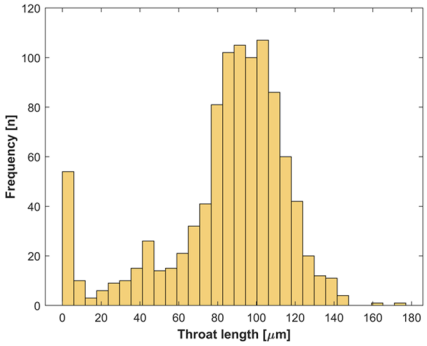

(b) Pore throat length

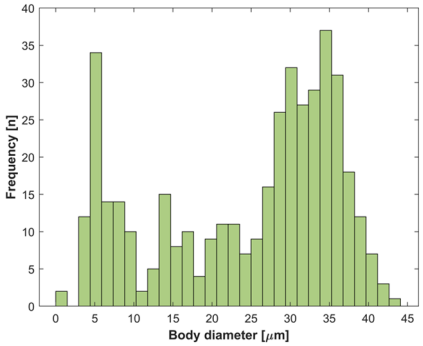

(c) Pore body diameter

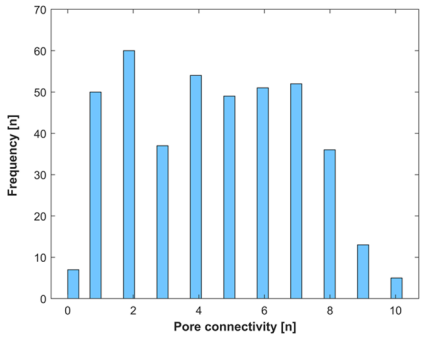

(d) Pore connectivity

Fig. 3 Results of pore extraction

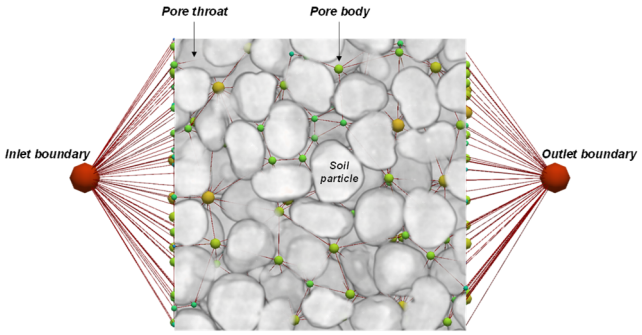

Fig. 4 Extracted pore network with boundary conditions

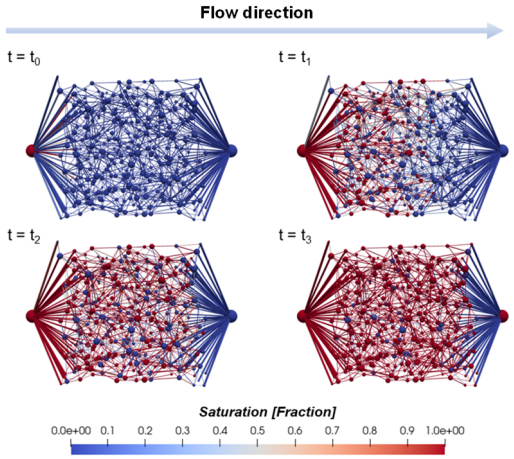

Fig. 5 Penetration behavior of biopolymer solution into pore network

resident fluids derived from the pore network extraction results. To establish the boundary conditions, the inlet and outlet ports were positioned at the coordinates obtained from the pore network, with the inlet port linked to the pore bodies in the first column, and the outlet port linked to those in the last column. Furthermore, all the pores were assumed to be 100% saturated with water to describe the permeation grouting condition.

The pressure distribution across all the pore bodies within the network is essential for calculating the flow rate. The mass balance equation (Eq. (1)) is expressed as a conductance matrix according to the Hagen–Poiseuille equation, excluding the pressure differential (Eq. (2)). Previous studies have suggested that biopolymers exhibit viscosity characteristics that are suitable for the power-law mathematical model of non-Newtonian fluids (Ryou and Jung 2023). Therefore, to accommodate non-Newtonian viscosity characteristics, apparent viscosity was calculated using Eq. (3) (Lenk 1978, Eberhard *et al*. 2019). Moreover, to consider the geometric properties of the pore throats connected to adjacent pore bodies, the effective conductance matrix was computed based on a half pore/ throat/half pore configuration using Eq. (4) (Xu *et al*. 2022).

$$q_i = \sum_{j=1}^{N} c_{ij}\left(P_j - P_i\right) = 0 \tag{1}$$

$$c_{ij} = \frac{\pi r^4}{8(\mu_i L_i + \mu_d L_d)} \tag{2}$$

$$\mu_{power-law} = k\frac{3n+1}{4n}\left(\frac{r\Delta P}{2kL}\right)^{\frac{n-1}{n}} \tag{3}$$

$$\frac{1}{c_{ij}} = \frac{1}{c_i} + \frac{1}{c_{t,ij}} + \frac{1}{c_j} \tag{4}$$

Here, q_i represents the conductance matrix, c_{ij} denotes the effective conductance matrix between pores i and j, P_j is the pressure at pore j, P_i is the pressure at pore i, r is the radius of the pore throat, μ is the viscosity, L is the length of the pore throat, $\mu_{\text{power-law}}$ is the viscosity of the power-law fluid, k is the consistency index, n is the behavior index, ΔP is the pressure difference, and $c_{t,ij}$ represents the conductance matrix of the pore throat between pores i and j.

Applying the mass balance equation to each pore body yields a single equation that considers the conductance matrix connected to other pore bodies and pore throats. Subsequently, all the equations for the unknown pressures in each pore body can be represented as a single matrix. Moreover, the previously determined boundary matrix allows the matrix representing pore bodies with unknown pressures to be expressed in the form of linear equations. In this study, the solution of the linear equations was computed to determine the pressure in all the pore bodies. After computing the pressure in all pore bodies, the fluid flow was simulated. Once all injected fluids were introduced into a single pore throat, the sequence was terminated. Subsequently, with each fluid injection, a new conductance matrix was generated, and the process of calculating the pressure in the new pore bodies and fluid flow occurrence was repeated. Finally, the pore network modeling concluded when the injected fluid reached the last column, no flow occurred.

Fig. 5 shows an example of the penetration behavior of a 2% agar gum solution within the pore network over time. In the figure, blue represents the resident fluid, that is, water, and red represents the injected fluid, that is, the 2% agar gum solution. The 2% agar gum solution exhibits stable injection behavior owing to its increased viscosity and capillary forces (Ryou and Jung 2023). Therefore, the penetration length of the 2% agar gum solution refers to the distance between the pore where the injection started and the pore where the injection concluded.

In this study, the injection characteristics of the biopolymers were analyzed based on their concentrations and pore sizes. For concentration-dependent analysis, the biopolymer solution exhibits shear-thinning behavior, where its apparent viscosity decreases with increasing shear rate. Among various models, including Power-law, Casson, Sisko, and Cross, regression analysis showed that the Power-law model had the highest accuracy in representing this behavior. Therefore, this study utilizes the Power-law parameters to model the viscosity characteristics of the biopolymer solution at different concentrations reported by Ryou and Jung (2023) were used. The analytical conditions are listed in Table 2.

For the analysis based on pore size, various pore-size

Table 2 Summary of pore network modeling cases with variations in biopolymer concentration

Case	Concentration [%]	Viscosity parameters		Injection pressure [Pa]
		Flow consistency index	Flow behavior index	
1	0.5	0.003	0.9866	0.1, 0.5, 1, 5
2	1.0	0.021	0.9168	0.5, 1, 5, 10
3	1.5	0.031	0.8870	0.5, 1, 5, 10
4	2.0	0.046	0.8511	1, 5, 10, 50

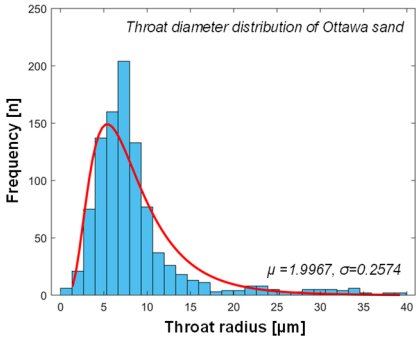

(a) Application of log-normal distribution based on Ottawa 20-30 sand

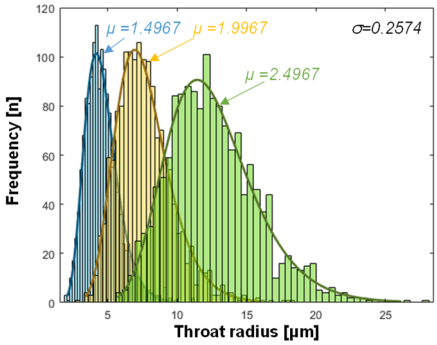

(b) Pore-size distribution generation according to mean of log-normal distribution

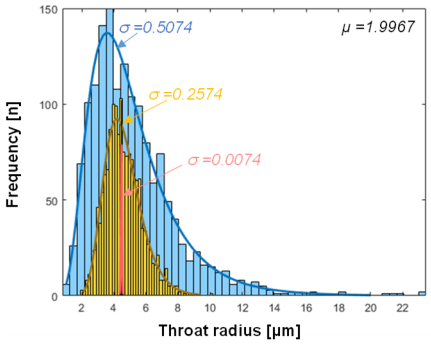

(c) Pore-size distribution generation according to standard deviation of log-normal distribution

Fig. 6 Generation of pore-size distributions

distributions were simulated. In the pore network model, flud flow is predominantly influenced by the size of the pore throats. Previous research has used log-normal

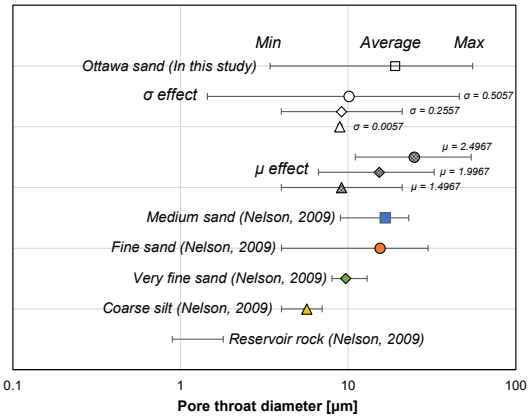

Fig. 7 Range of pore throat diameters by soil type

Table 3 Summary of pore network modeling cases with variations in pore-size distribution

Case	Injection pressure [Pa]	Log-normal distribution	
		μ	σ
1	1, 5, 10, 50	1.4967	0.2574
2	1, 5, 10, 50	1.9967	0.2574
3	1, 5, 10, 50	2.4967	0.2574
4	1, 5, 10, 50	1.4967	0.0074
5	1, 5, 10, 50	1.4967	0.5074

distributions to quantify the distribution of pore throat sizes (Cao *et al.* 2016). Fig. 6 illustrates the creation of pore networks to simulate various pore-size distributions. Fig. 6(a) shows the application of a log-normal distribution to the pore throat sizes of Ottawa 20-30 sand, whereas Figs. 6(b) and (c) illustrate the changes in the mean size and standard deviation of the log-normal distribution, respectively. The mean and standard deviation results of the log-normal distribution of Ottawa 20-30 sand were 1.9967 and 0.2574, respectively. Based on these parameters, three different sets of mean and standard deviation values were used to generate various pore-size distributions.

To determine reasonable mean and standard deviation values for the log-normal distribution, we compared the pore throat diameters that were reported in previous studies. Fig. 7 shows a schematic of the distribution of pore throat diameters for different soil types (Nelson 2009). Our analysis revealed that the pore-size distribution of the Ottawa sand used in this study resembles that of medium sand, but with a broader distribution. The sand with pore throat sizes with a smaller mean (μ = 1.4967) approach the size of very fine sand, but with a wider distribution. Those with a medium mean size (μ = 1.9967) were observed to be similar overall to the pore sizes of fine sand. The largest mean size (μ = 2.4967) exceeded the average size and distribution of medium sand.

A comparison of the distributions based on the standard deviation indicated that the mean sizes ranged from those of very fine to fine sand, and variations in the distribution width were observed. Hence, the Ottawa sand used in this study can be characterized as having a broad distribution

similar to medium sand, with distributions in terms of mean size resembling those of very fine, fine, and medium-coarse sands, depending on the mean. Distributions based on the standard deviation suggest variability, ranging from poor to good particle size distribution of very fine sand. Simulations of pore throat size distributions, influenced by the mean and standard deviation, were conducted using a 2% agar gel solution, with connectivity and pore locations identical to Ottawa 20-30 sand. These conditions are listed in Table 3.

4. Results

The pore network modeling performed in this study included pore extraction and fluid flow simulations.

4.1 Effect of biopolymer concentration on injection characteristics

Fig. 8 shows the penetration distance as a function of the concentration. As the concentration of the agar gel solution increases, an evident overall decrease in the penetration length can be observed. This decrease is more pronounced at lower pressures, such as 0.5 and 1 Pa, where the viscosity effects of the polymer significantly limit its penetration ability. In contrast, at higher pressures, such as 5 and 10 Pa, the decrease in penetration length is relatively gradual, suggesting that high pressure can overcome the viscosity resistance of the polymer. However, as the pressure increases, the rate of decrease in the penetration length at high concentrations gradually decreases, indicating that the increased viscosity at high concentrations substantially reduces the permeability.

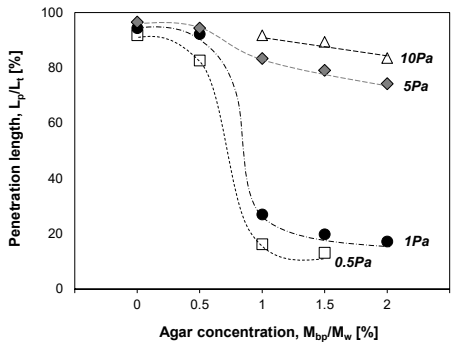

Fig. 8 Effect of agar concentration on penetration length

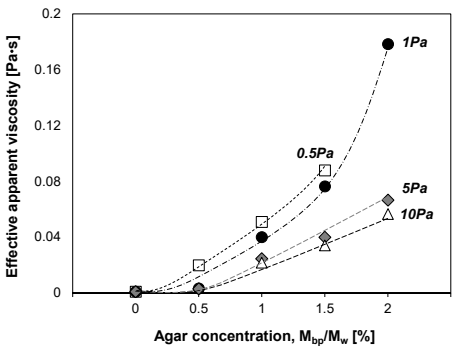

Fig. 9 Effect of agar concentration on effective apparent viscosity

Fig. 9 illustrates the variation in the average apparent viscosity as a function of concentration. The effective apparent viscosity represents the average of the effective apparent viscosities of all the fluids within the pore network. The effective apparent viscosity consistently increases at all pressure levels as the agar gel concentration increases. The increase in viscosity indicates increased interactions between the polymer chains and higher internal friction, which impedes fluid flow. This increase in viscosity is particularly significant at lower pressures, such as 0.5 and 1 Pa, thus requiring higher pressures for flow in high-concentration polymer solutions. Moreover, as the injection pressure increases within the same concentration of the agar gel solution, the effective apparent viscosity also increases. This reflects the shear-thinning characteristics of the agar gel solution, where an increase in injection pressure reduces the effective apparent viscosity, potentially further enhancing the permeability.

4.2 Effect of pore-size distribution on injection characteristics

Fig. 10 illustrates the injection characteristics according to the pore-size distribution. Figs. 10(a) and (b) show the penetration lengths and effective apparent viscosities according to the mean of the log-normal distribution, respectively, whereas Figs. 10(c) and (d) show these properties according to the standard deviation of the log-normal distribution, respectively. The penetration length increases with the mean of the log-normal distribution across all pressure conditions, indicating that larger average pore sizes allow more space for fluid movement, thereby facilitating fluid flow. This effect is particularly emphasized under high-pressure conditions (50 Pa), where fluids can traverse larger pores more effectively. As the pressure increases from 1 to 50 Pa, the rate of increase in the penetration length also increases, indicating that higher pressures can more effectively overcome the resistance between pores. As the mean increases, the effective apparent viscosity decreases owing to the enhanced fluid dynamics and reduced internal friction, particularly at low pressures, where high viscosities manifest in small penetration lengths.

As the standard deviation of the log-normal distribution increases, the penetration length also increased. A larger standard deviation implies a wider distribution of pore sizes, implying that both small and large pores coexist, allowing fluids to move more easily through large pores and offering multiple pathways for fluid movement through pores of various sizes. This variation in pore size decreases the overall viscosity because diverse pathways facilitate easier fluid movement. Moreover, the presence of pores of varying sizes induces different hydrodynamic interactions, which improve the overall flow of the fluid.

5. Discussion

The methodology for the geotechnical application of biopolymers that has been conceptualized in this study

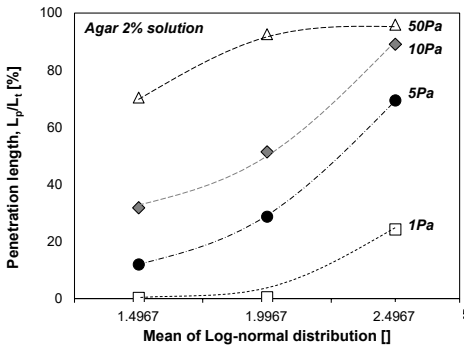

(a) Effect of μ on penetration length

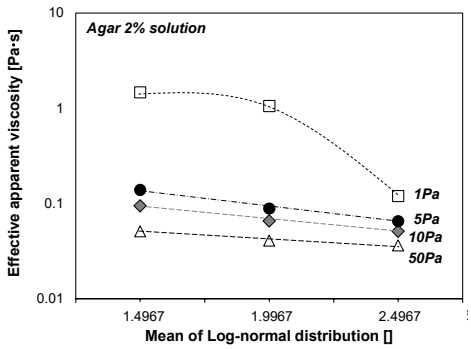

(b) Effect of μ on effective apparent viscosity

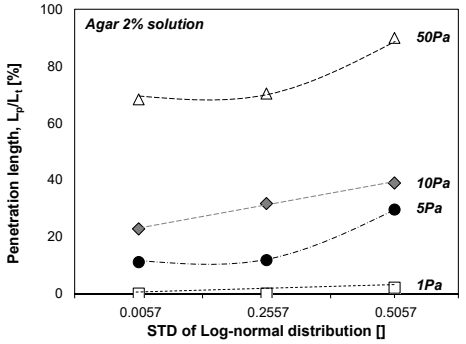

(c) Effect of σ on penetration length

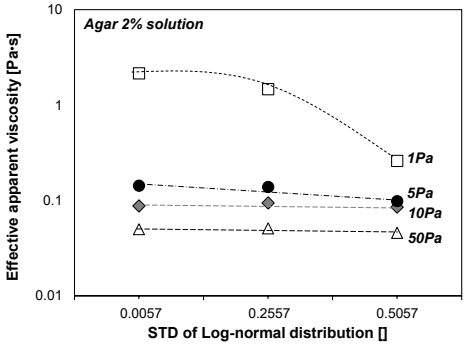

(d) Effect of σ on effective apparent viscosity

Fig. 10 Effect of pore-size distribution on injection characteristics

involves their use as grouting materials. Permeation grouting, a technique among grouting methods, involves injecting and solidifying material within pores without causing deformation of the ground, thus improving the soil structure. The injection characteristics of the fluids in the permeation grouting method follow the theory of fluid flow within the pores. This section analyzes these characteristics based on the theory of fluid flow in pores, as reported in Section 4, and includes a quantitative analysis based on upscaling methods for field applications.

The various factors influencing the fluid flow within the pores are illustrated in Fig. 11. These factors include the physicochemical properties of the fluid, geometric characteristics of the pores, and injection and ground conditions. The physicochemical properties of a fluid, including its viscosity, density, interfacial tension, and wettability, play crucial roles in determining its flow and interaction (Hirasaki and Lawson 1985, Czachor *et al.* 2010). The geometric characteristics of pores, such as size, shape, distribution, connectivity, and curvature, directly affect the effective movement of fluids within the soil (Doyen 1988, Hu *et al.* 2012, Imani *et al.* 2022).

The injection and ground conditions, including the injection pressure, injection rate, soil saturation, and permeability, are key determinants of the efficiency of the injection process (van Genuchten and Jury 1987, Wanniarachchi *et al.* 2017, Assilzadeh *et al.* 2021). In this study, the target ground was assumed to be saturated with water. Viscosity was considered among the physicochemical properties. Because the agar gel solution was a water-based solution, density changes were assumed to be negligible. Furthermore, because the agar gel solution and water form

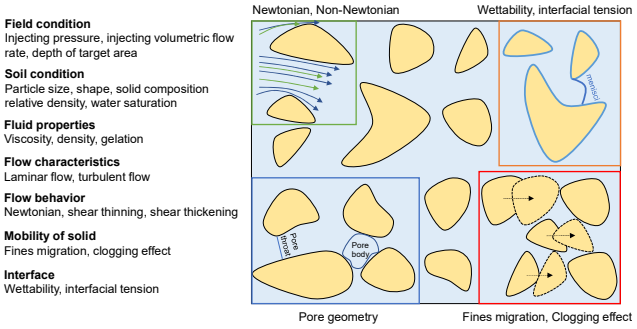

Fig. 11 Factor affecting fluid flow in porous media

a homogeneous fluid, resistance at the interface was not considered. The geometric characteristics of the pores were analyzed using the same samples; therefore, no differences in the geometric properties were assumed. The injection pressure was considered in the injection and ground conditions, and the soil saturation was assumed to be 100%. Consequently, under the simulation conditions of this study, the viscosity and injection pressure were identified as the primary factors affecting the fluid flow within the pores.

5.1 Effect of viscosity and injection pressure on injection characteristics

Fig. 12 illustrates the relationship between the injection pressure, distance, and apparent viscosity, following the logic presented in the previous section. The apparent viscosity was determined based on the concentration of the agar gel solution and injection pressure and was set to

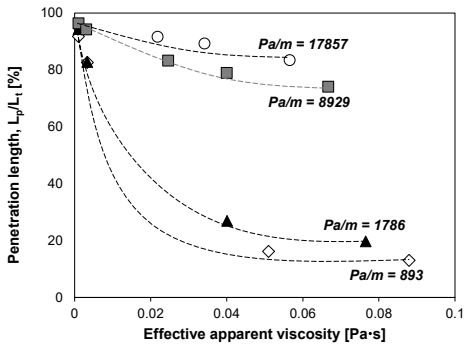

Fig. 12 Relation between effective apparent viscosity, penetration length, and pressure gradient

a single value irrespective of the agar concentration. The pressure gradient represents the pressure required to inject fluid to a distance of 1 m. The analysis showed that as the effective apparent viscosity increases, the penetration length evidently decreases. This is because a higher viscosity increases the internal friction of the fluid, which requires more energy to pass through the pores. As viscosity varies within the range of 0.01 to 0.1 Pa·s, the penetration length decreases from approximately 100% to as low as approximately 20%. Changes according to the pressure gradient show that, at high pressure gradients, the penetration length tends to be longer, suggesting that high pressure helps to overcome the resistance caused by viscosity and pushes the fluid even further. For example, at a pressure gradient of 17,857 Pa/m, the penetration length remains relatively high despite the increase in viscosity. In contrast, at a pressure gradient of 893 Pa/m, an increase in viscosity resulted in a more pronounced decrease in the penetration length, indicating that viscosity has a more decisive effect on penetration at lower pressure gradients.

Through this analysis, the agar gel solution could be considered as a fluid expressing a single apparent viscosity, irrespective of the concentration, and the penetration distance was analyzed based on this viscosity under varying injection pressures. The analysis suggests that the viscosity characteristics of the injected fluid and injection pressure can determine the penetration distance. However, this analysis was conducted on a limited sizes of Ottawa 20-30 sand, and upscaling considering the size of the actual ground is required. This aspect is discussed in Section 5.3.

5.2 Effect of pore throat size distribution on injection characteristics

Changes in the mean and standard deviation of the pore throat sizes can be considered as indicators of the size and distribution quality of the soil particles. Based on the determined means and standard deviations, soil classification was performed. Fig. 13 illustrates the injection characteristics related to the soil particle distribution and classification, which were obtained using only a 2% agar gel solution and were based on the aforementioned assumptions. The analysis shows that well-graded soils, which have particles of various sizes, and therefore, more pore space, exhibit higher penetration distances. Conversely, poorly graded soils with uniformly sized particles have smaller pore spaces, and consequently, the shortest penetration distances.

The analysis of penetration distances based on soil type showed that very fine sand, which comprises fine particles, resulted in limited penetration distance, whereas the larger particle sizes present in medium-coarse and well-graded soils tended to increase penetration distances. This is because the larger gaps between larger particles facilitate fluid movement. Both effects demonstrated that the penetration distances increased at higher injection pressures. The highest penetration distances were observed at 50 Pa, indicating that high pressure can forcefully inject the fluid further, particularly in well-graded soils, where large pores significantly enhance the effect of pressure.

These results indicate that the penetration capability of biopolymer solutions is highly dependent on the physical properties of the soil, suggesting that optimal injection conditions must consider soil particle distribution and type. By adjusting the injection pressure, effective penetration can be achieved across various ground conditions, and these data can be utilized as essential foundational information for engineering applications, such as ground reinforcement or remediation. However, this study classified soils based merely on the range of pore throat sizes owing to insufficient reported data. Therefore, future studies should build a database based on the pore structure analysis of

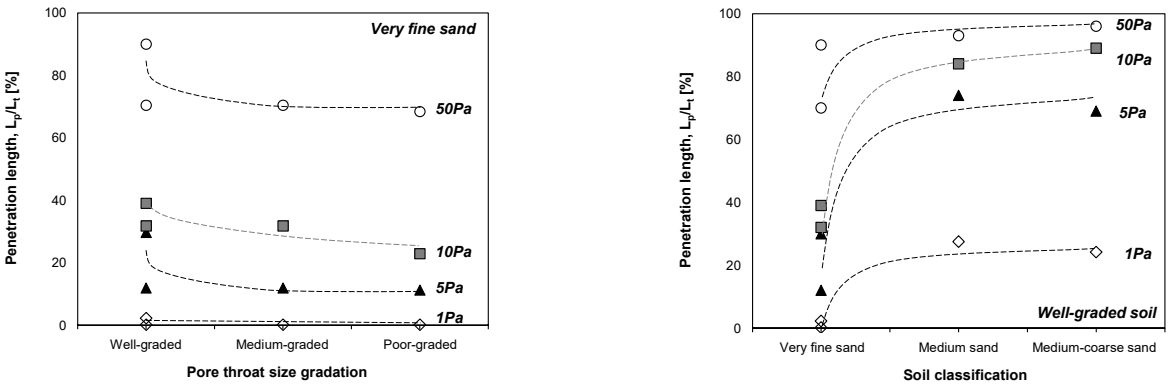

(a) Effect of size gradation on penetration length

(b) Effect of soil type on penetration length

Fig. 13 Effect of pore-size distribution on injection characteristics

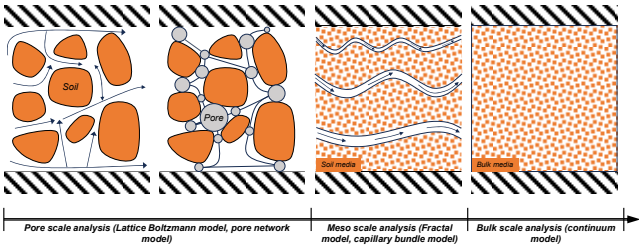

Fig. 14 Various numerical techniques to assess fluid flow in porous media according to scale

various samples.

5.3 Upscaling to assess injection characteristics of biopolymer solution

Fig. 14 shows a schematic of a numerical study for analyzing the fluid flow within pores, categorized into pore-, meso-, and bulk-scale analyses based on the scale of the analyzed ground. The pore-scale approach includes the models used in this study, such as the pore network and lattice Boltzmann models. The mesoscale approach encompasses models such as the fractal and capillary bundle models, whereas the bulk-scale approach is represented by continuum models. Pore-scale analysis focuses on the geometric shape of pores and flow of small-scale particles, offering relatively high accuracy within this scope by minimizing errors due to soil heterogeneity. However, it requires a large amount of data and significant amount of calculation time, making it less practical for field-scale applications.

In contrast, the bulk-scale approach simplifies the analysis by treating the soil heterogeneity, including the geometric shape of the pores, as a single parameter. This allows for a relatively straightforward analysis at the field scale but tends to be less accurate because of the simplified representation of the actual state of the ground. In this study, a pore throat enhancement technique was employed for field-scale injection prediction using pore network modeling. This technique involves increasing the length of the pore throats to enhance the overall size of a pore network that has size limitations, allowing small-scale pore networks to be expanded to mesoscale models such as the fractal or capillary bundle models. The pore network of the Ottawa sand used in this study typically exhibits a length of approximately 4.5 mm; however, all pore throats within the network were enhanced 100 times to simulate a network of approximately 4.5 m in length.

Fig. 15 illustrates the changes in the penetration length as influenced by the effective apparent viscosity and injection pressure. This study simulated the injection of a Newtonian fluid and 2% agar solution at pressures of 35, 100, 200, and 300 kPa. The penetration-length prediction model was validated by comparison with previous data and analysis results for Newtonian fluids with viscosities of 0.01, 0.05, 0.1, 0.15, and 0.2 Pa·s. The previous data corresponded to the penetration lengths according to the effective apparent viscosities and injection pressures of fluids following the Bingham model and Newtonian fluids, all of which were recalibrated to effective apparent

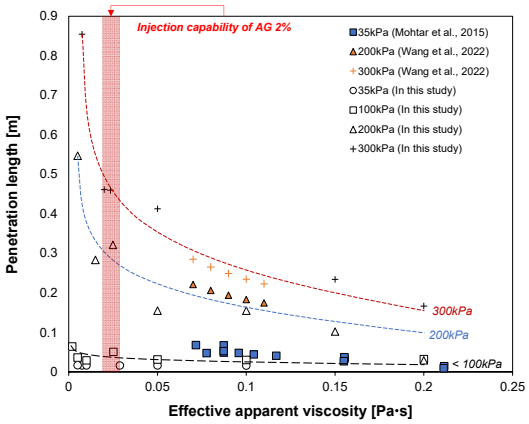

Fig. 15 Effect of effective apparent viscosity and injection pressure on the penetration length (El Mohtar *et al*. 2015, Wang *et al*. 2022)

viscosity values from the literature (El Mohtar *et al*. 2015, Wang *et al*. 2022).

The analysis revealed that, at the same injection pressure, an increase in the effective apparent viscosity led to a reduction in the penetration length. Moreover, at the same effective apparent viscosity, an increase in the injection pressure resulted in an increased penetration length. For the 2% agar injection, the effective apparent viscosity values ranged between 0.0228 and 0.02 Pa·s depending on the injection pressure, showing a 15% decrease in viscosity with increasing pressure. Comparing these results with previous data, no clear change in the penetration length owing to viscosity was observed at pressures below 100 kPa, which was probably because the low pressure was insufficient to effectively move the fluid. However, at an injection pressure of 200 kPa, a clear decrease in penetration length was observed with increasing viscosity. Moreover, at pressures above 200 kPa, a logarithmic trend was observed, and previous data and analysis results for the same effective apparent viscosity showed similar values.

This analysis suggests that reducing the effective apparent viscosity of the injected fluid and increasing the injection pressure can increase the penetration length of the injection material. Finally, the developed model and results led to the derivation of a meaningful relationship formula that could be used to calculate the penetration distance based on the viscosity and injection pressure of both Newtonian and non-Newtonian fluids, including biopolymer solutions.

6. Conclusions

This study analyzed a pore network model-based approach to investigate the injection characteristics of biopolymer solutions. The conclusions drawn from the study are as follows.

- In this study, original images of Ottawa 20-30 sand were utilized to construct a pore network effectively. The construction process required image processing and a threshold setting. The structural characteristics

of the pores were quantified using maximal ball and medial axis algorithms, resulting in the establishment of a pore network. During the modeling process, the modified Hagen–Poiseuille equation was used to simulate the flow of non-Newtonian fluids, presenting an advanced approach that considers the characteristics of non-Newtonian fluids, which were overlooked by previous models.

- In the injection analysis with the agar gel solution, an increase in concentration was observed to lead to a higher viscosity and reduced injectability. This occurs because the increase in fluid viscosity owing to higher concentrations acts as a primary factor in reducing injectability. However, increasing the injection pressure improved injectability owing to the shear-thinning behavior of the agar solution, which reduced the apparent viscosity of the fluid. These results suggest that an appropriate adjustment of the injection pressure can significantly enhance grouting efficiency in the field.
- The size distribution of the pore throats was analyzed based on data extracted from Ottawa sand. The analysis indicated that both the average size and the distribution of pore throat sizes significantly affected the flow of the injection material, with increases in the average pore-throat size and a favorable particle size distribution resulting in improved injectability. This provides an important benchmark for quantitatively understanding the impact of pore-throat size characteristics on fluid flow. However, as this analysis was based on limited data, future studies require a sufficient database size that can be obtained through experiments with various samples and conditions.
- The accuracy of the developed pore network model was evaluated through a comparative analysis with laboratory experimental results. Similar trends observed in the penetration distance with respect to injection pressure and fluid viscosity enhanced the reliability of the model, indicating its applicability under real field conditions. This model can also be effectively used to analyze the flow characteristics of Newtonian and non-Newtonian fluids within pores.
- In conclusion, this study offers a new methodology for constructing pore networks and understanding fluid flow characteristics, which could contribute to the development and optimization of injection materials, such as permeation grouting. Moreover, the findings of this study are expected to play a crucial role in providing a technical foundation for improving the efficiency of grouting operations in the field.

Acknowledgments

This work was supported by the National Research Foundation of Korea (NRF) grant funded by the Korean Government (MSIT), (2022R1A4A3029737) (RS-2024-00353644).

References

Arab, M.G., Mousa, R.A., Gabr, A.R., Azam, A.M., El-Badawy, S.M. and Hassan, A.F. (2019), "Resilient behavior of sodium alginate–treated cohesive soils for pavement applications", *J. Mater. Civil Eng.*, 31(1), 04018361. https://doi.org/10.1061/(ASCE)MT.1943-5533.0002565

Assilzadeh, H., He, Y., Alyousef, R., Alaskar, A., Alabduljabbar, H., Mohamed, A.M., Maureira-Carsalade, N., Roco-Videla, A. and Issakhov, A. (2021), "Influence of crack on the permeability of plastic concrete", *Smart Struct. Syst., Int. J.*, **27**(5), 871-890. https://doi.org/10.12989/sss.2021.27.5.871

Baranwal, A., Yadav, A. and Gupta, S. (2021), "A comparative case study on various admixtures used for soil stabilization", *Soil Dyn.: Sel. Proc. 7th ICRAGEE 2020*, pp. 147-157.

Bouazza, A., Gates, W.P. and Ranjith, P.G. (2009), "Hydraulic conductivity of biopolymer-treated silty sand", *Géotechnique*, **59**(1), 71-72. https://doi.org/10.1680/geot.2007.00137

Butt, W.A., Gupta, K. and Jha, J.N. (2016), "Strength behavior of clayey soil stabilized with saw dust ash", *Int. J. Geo-Eng.*, **7**(1), 1-9. https://doi.org/10.1186/s40703-016-0032-9

Cao, S.C., Dai, S. and Jung, J. (2016), "Supercritical CO2 and brine displacement in geological carbon sequestration: Micromodel and pore network simulation studies", *Int. J. Greenh. Gas Control*, **44**, 104-114. https://doi.org/10.1016/j.ijggc.2015.11.026

Čapek, M., Janáček, J. and Kubínová, L. (2006), "Methods for compensation of the light attenuation with depth of images captured by a confocal microscope", *Microsc. Res. Tech.*, **69**(8), 624-635. https://doi.org/10.1002/jemt.20330

Chang, I. and Cho, G.C. (2019), "Shear strength behavior and parameters of microbial gellan gum-treated soils: from sand to clay", *Acta Geotech.*, **14**, 361-375. https://doi.org/10.1007/s11440-018-0641-x

Chen, P.C., Yu, C.H., Surjanto, Y.K., Peng, S.K. and Chang, K.C. (2022), "Numerical modelling of a shear-thickening fluid damper using optimal transit parameters", *Smart Struct. Syst., Int. J.*, **30**(5), 447-462. https://doi.org/10.12989/sss.2022.30.5.447

Coskun, S.B. and Tokdemir, T. (2020), "Modelling of permeation grouting through soils", *J. Appl. Eng. Sci.*, **10**(1), 11-16. https://doi.org/10.2478/jaes-2020-0003

Czachor, H., Doerr, S.H. and Lichner, L. (2010), "Water retention of repellent and subcritical repellent soils: New insights from model and experimental investigations", *J. Hydrol.*, **380**(1-2), 104-111. https://doi.org/10.1016/j.jhydrol.2009.10.027

Dong, H. and Blunt, M.J. (2009), "Pore-network extraction from micro-computerized-tomography images", *Phys. Rev. E*, **80**(3), 036307. https://doi.org/10.1103/PhysRevE.80.036307

Doyen, P.M. (1988), "Permeability, conductivity, and pore geometry of sandstone", *J. Geophys. Res.: Solid Earth*, **93**(B7), 7729-7740. https://doi.org/10.1029/JB093iB07p07729

Eberhard, U., Seybold, H.J., Floriancic, M., Bertsch, P., Jiménez-Martínez, J., Andrade Jr, J.S. and Holzner, M. (2019), "Determination of the effective viscosity of non-Newtonian fluids flowing through porous media", *Front. Phys.*, **7**, 71. https://doi.org/10.3389/fphy.2019.00071

El Mohtar, C.S., Yoon, J. and El-Khattab, M. (2015), "Experimental study on penetration of bentonite grout through granular soils", *Can. Geotech. J.*, **52**(11), 1850-1860. https://doi.org/10.1139/cgj-2014-0422

Fatehi, H., Ong, D.E., Yu, J. and Chang, I. (2021), "Biopolymers as green binders for soil improvement in geotechnical applications: A review", *Geosci.*, **11**(7), 291. https://doi.org/10.3390/geosciences11070291

Fei, W., Narsilio, G.A., van der Linden, J.H., Tordesillas, A., Disfani, M.M. and Santamarina, J.C. (2021), "Impact of particle

shape on networks in sands", *Comput. Geotech.*, **137**, 104258. https://doi.org/10.1016/j.compgeo.2021.104258

Firoozi, A.A., Guney Olgun, C., Firoozi, A.A. and Baghini, M.S. (2017), "Fundamentals of soil stabilization", *Int. J. Geo-Eng.*, **8**(1), 1-16. https://doi.org/10.1186/s40703-017-0064-9

Fu, Y., Wang, X., Zhang, S. and Yang, Y. (2019), "Modelling of permeation grouting considering grout self-gravity effect: Theoretical and experimental study", *Adv. Mater. Sci. Eng.*, **2019**, 1-16. https://doi.org/10.1155/2019/7968240

Gidebo, F.A., Yasuhara, H. and Kinoshita, N. (2023), "Stabilization of expansive soil with agricultural waste additives: a review", Int. *J. Geo-Eng.*, **14**(1), 14. https://doi.org/10.1186/s40703-023-00194-x

Hirasaki, G.J. and Lawson, J.B. (1985), "Mechanisms of foam flow in porous media: apparent viscosity in smooth capillaries", *Soc. Pet. Eng. J.*, **25**(02), 176-190. https://doi.org/10.2118/12129-PA

Hu, Q., Ewing, R.P. and Dultz, S. (2012), "Low pore connectivity in natural rock", *J. Contam. Hydrol.*, **133**, 76-83. https://doi.org/10.1016/j.jconhyd.2012.03.006

Imani, M., Nejati, H.R., Goshtasbi, K. and Nazerigivi, A. (2022), "Effect of brittleness on the micromechanical damage and failure pattern of rock specimens", *Smart Struct. Syst., Int. J.*, **29**(4), 535-547. https://doi.org/10.12989/sss.2022.29.4.535

Jerez Lazo, C., Lee, N., Tripathi, P., Joykutty, L., Jayachandran, K. and Lee, S.J. (2024), "A fungus-based soil improvement using Rhizopus oryzae inoculum", *Int. J. Geo-Eng.*, **15**(1), 18. https://doi.org/10.1186/s40703-024-00218-0

Jerez Lazo, C., Lee, N., Tripathi, P., Joykutty, L., Jayachandran, K. and Lee, S.J. (2024), "A fungus-based soil improvement using Rhizopus oryzae inoculum", *Int. J. Geo-Eng.*, **15**(1), 18. https://doi.org/10.1186/s40703-024-00218-0

Jithin, M., Kumar, N., De, A. and Das, M.K. (2018), "Pore-scale simulation of shear thinning fluid flow using lattice boltzmann method", *Transp. Porous Media*, **121**, 753-782. https://doi.org/10.1007/s11242-017-0984-z

Kim, R.E., Koh, E. and Jin, S.S. (2022), "Physical interpretation of concrete crack images from feature estimation and classification", *Smart Struct. Syst., Int. J.*, **30**(4), 385-395. https://doi.org/10.12989/sss.2022.30.4.385

Lee, M., Im, J., Chang, I. and Cho, G.C. (2021), "Evaluation of injection capabilities of a biopolymer-based grout material", *Geomech. Eng., Int. J.*, **25**(1), 31-40. https://doi.org/10.12989/gae.2021.25.1.031

Lee, J., Kim, K., Kim, H. and Sohn, H. (2024), "Coating defect classification method for steel structures with vision–thermography imaging and zero-shot learning", *Smart Struct. Syst., Int. J.*, **33**(1), 55. https://doi.org/10.12989/sss.2024.33.1.055

Lenk, R.S. (1978), "The Hagen-Poiseuille equation and the Rabinowitsch correction. The pressure drop in tapered channels", *Polym. Rheol.*, 75-85. https://doi.org/10.1007/978-94-010-9666-97

Li, Y., Alves, R., Vanapalli, S., Gitirana Jr, G. (2024), "Models for considering the thermo-hydro-mechanical-chemo effects on soil–water characteristic curves", *Geosci.*, **14**(2), 38. https://doi.org/10.3390/geosciences14020038

Mekonnen, E., Amdie, Y., Etefa, H., Tefera, N. and Tafesse, M. (2022), "Stabilization of expansive black cotton soil using bioenzymes produced by ureolytic bacteria", *Int. J. Geo-Eng.*, **13**(1), 10. https://doi.org/10.1186/s40703-022-00175-6

Nelson, P.H. (2009), "Pore-throat sizes in sandstones, tight sandstones, and shales", *AAPG Bull.*, **93**(3), 329-340. https://doi.org/10.1306/10240808059

Pushpakumara, B.H.J. and Mendis, W.S.W. (2022), "Suitability of rice husk ash (RHA) with lime as a soil stabilizer in geotechnical applications", *Int. J. Geo-Eng.*, **13**(1), 4. https://doi.org/10.1186/s40703-021-00169-w

Ryou, J.E. and Jung, J. (2022), "Penetration behavior of biopolymer aqueous solutions considering rheological properties", *Geomech. Eng., Int. J.*, **29**(3), 259-267. https://doi.org/10.12989/gae.2022.29.3.259

Ryou, J.E. and Jung, J. (2023), "Characteristics of thermo-gelation biopolymer solution injection into porous media", *Constr. Build. Mater.*, **384**, 131451. https://doi.org/10.1016/j.conbuildmat.2023.131451

Seo, S., Lee, M., Im, J., Kwon, Y.M., Chung, M.K., Cho, G.C. and Chang, I. (2021), "Site application of biopolymer-based soil treatment (BPST) for slope surface protection: In-situ wet-spraying method and strengthening effect verification", *Constr. Build. Mater.*, **307**, 124983. https://doi.org/10.1016/j.conbuildmat.2021.124983

Sochi, T. (2010), "Flow of non-Newtonian fluids in porous media", *J. Polym. Sci. Part B: Polym. Phys.*, **48**(23), 2437-2767. https://doi.org/10.1002/polb.22144

Soldo, A., Miletić, M. and Auad, M.L. (2020), "Biopolymers as a sustainable solution for the enhancement of soil mechanical properties", *Sci. Rep.*, **10**(1), 267. https://doi.org/10.1038/s41598-019-57135-x

Toufigh, V. and Ghassemi, P. (2020), "Control and stabilization of fugitive dust: Using eco-friendly and sustainable materials", *Int. J. Geomech.*, **20**(9), 04020140. https://doi.org/10.1061/(ASCE)GM.1943-5622.0001762

van Genuchten, M.T. and Jury, W.A. (1987), "Progress in unsaturated flow and transport modeling", *Rev. Geophys.*, **25**(2), 135-140. https://doi.org/10.1029/RG025i002p00135

Wang, X., Cheng, H., Yao, Z., Rong, C., Huang, X. and Liu, X. (2022), "Theoretical research on sand penetration grouting based on cylindrical diffusion model of tortuous tubes", *Water*, **14**(7), 1028. https://doi.org/10.3390/w14071028

Wanniarachchi, W.A.M., Ranjith, P.G. and Perera, M.S.A. (2017), "Shale gas fracturing using foam-based fracturing fluid: a review", *Environ. Earth Sci.*, **76**, 1-15. https://doi.org/10.1007/s12665-017-6399-x

Xiong, Q., Baychev, T.G. and Jivkov, A.P. (2016), "Review of pore network modelling of porous media: Experimental characterisations, network constructions and applications to reactive transport", *J. Contam. Hydrol.*, **192**, 101-117. https://doi.org/10.1016/j.jconhyd.2016.07.002

Xu, K., Wei, W., Chen, Y., Tian, H., Xu, S. and Cai, J. (2022), "A pore network approach to study throat size effect on the permeability of reconstructed porous media", *Water*, **14**(1), 77. https://doi.org/10.3390/w14010077

Zivari, A., Siavoshnia, M. and Rezaei, H. (2023), "Effect of lime-rice husk ash on geotechnical properties of loess soil in Golestan province, Iran", *Int. J. Geo-Eng.*, **14**(1), 20. https://doi.org/10.1186/s40703-023-00199-6